# Lattice Boltzmann scheme for electrolytes by an extended Maxwell-Stefan approach

Jens Zudrop,[1,2,*] Sabine Roller,[1,2,†] and Pietro Asinari[3,‡]

[1]*Applied Supercomputing in Engineering, German Research School for Simulation Sciences, RWTH Aachen, Schinkelstrasse 2a, Aachen, Germany*

[2]*Simulation Techniques and Scientific Computing, University Siegen, Hölderlinstrasse 3, Siegen, Germany*

[3]*Department of Energy, Politecnico di Torino, Corso Duca degli Abruzzi 24, Torino, Italy*

(Received 4 February 2013; revised manuscript received 24 February 2014; published 19 May 2014)

This paper presents an extended multicomponent lattice Boltzmann model for the simulation of electrolytes. It is derived by means of a finite discrete velocity model and its discretization. The model recovers momentum and mass transport according to the incompressible Navier-Stokes equation and Maxwell-Stefan formulation, respectively. It includes external driving forces (e.g., electric field) on diffusive and viscous scales, concentration-dependent Maxwell-Stefan diffusivities, and thermodynamic factors. The latter take into account nonideal diffusion behavior, which is essential as electrolytes involve charged species and therefore nonideal long and short-range interactions among the molecules of the species. Furthermore, we couple our scheme to a finite element method to include electrostatic interactions on the macroscopic level. Numerical experiments show the validity of the presented model.

DOI: 10.1103/PhysRevE.89.053310 PACS number(s): 47.11.−j, 66.10.cg, 51.10.+y

## I. INTRODUCTION

In the past decade lattice Boltzmann models have become a popular numerical method to solve reduced kinetic models, in particular for the incompressible Navier-Stokes equation. In subsequent years it has been applied successfully to a number of complex problems in science and engineering [1–5]. A promising research area for lattice Boltzmann methods is multicomponent flows in complex geometries, e.g., porous media. In contrast to standard continuum-based models, e.g., Refs. [6,7], lattice Boltzmann algorithms are well suited for complex setups on high-performance computers. However, a straightforward extension of lattice Boltzmann BGK models to multicomponent flows fails due to the fact that a proper way of interaction between the species has to be defined in the kinetic formulation. In recent years a number of different models have emerged: Some models properly take into account the momentum exchange between the species by pseudopotential interactions [8–11]. Others have defined free energies [12–15], while still others [16,17] have adopted a force coupling in the momentum equations, derived from a linearized kinetic term and further [18–20] avoid a linearization by two collision operators. In Ref. [21] another LB scheme has been proposed aiming to minimize a proper H function defined on the fully discrete lattice.

Our work is a further extension of the models proposed in Refs. [20,22] (which are based on Ref. [23]). Therefore, it inherits most of the basic properties as the indifferentiability principle; its main idea is to exchange momentum among the species according to the Maxwell-Stefan formulation and the fact that the diffusion equations are recovered even when the mixture averaged diffusion approximation does not hold [24]. For further detailed comparison of existing models we refer the reader to the previously mentioned publications and references therein.

However, in this work a number of extensions for electrolytes and electrodialytic processes is presented: Compared to ideal mixtures, where any interaction between two species is the same, electrolytes show additional nonideal diffusion behavior (due to significant deviation from spherical molecule shape, variations in molecule size, long-range electrostatic interactions between molecules, and short-range van der Waals interactions) and thus only parts of the ionic species might be active. Even in diluted electrolytes the deviation from ideal behavior becomes apparent [25]. The Maxwell-Stefan closure relation incorporates these effects by use of the so-called thermodynamic factors [26], a coefficient matrix which is mathematically derived by the concept of activity coefficients. To the knowledge of the authors this is the first time that thermodynamic factors (and therefore nonideal diffusion processes) are considered in the context of mixture lattice Boltzmann models. Electric forces are the main driving force for convection and diffusion in electrolytes and electrodialysis processes, therefore we present a proper inclusion of these driving forces in our finite discrete velocity model (FDVM). In comparison to Ref. [22], our approach requires no additional correction terms, works in presence of thermodynamic factors, and is applicable in nonelectroneutral regimes, where strong diffusive driving forces apply (as long as the diffusive asymptotic limit is applied). Since the Maxwell-Stefan diffusivities for electrolytes show a significant dependence on species' concentrations [27], we consider variable diffusivities in our FDVM. The model recovers the governing conservation equations asymptotically in the diffusive limit [28,29]. The correct nonlinear hydrodynamic mixture behavior is recovered, even in regimes where diffusion velocities are large (and mixture velocity is small). Furthermore, our model recovers the Maxwell-Stefan equations in terms of molar quantities (which is more common for electrolytes) and it avoids the utilization of nondefined quantities for liquid electrolytes (e.g., partial pressures, etc.).

*Author to whom correspondence should be addressed: j.zudrop@grs-sim.de

†sabine.roller@uni-siegen.de

‡pietro.asinari@polito.it

 ©2014 American Physical Society

This paper is structured as follows: In Sec. II we present the equations of motion for an electrolyte solution. Section III presents a simplified kinetic model, a FDVM, that recovers the equations of motion for an electrolyte asymptotically. Section IV provides simulation results of a fully discrete lattice Boltzmann scheme derived by integrating the FDVM along its characteristics. Finally, Sec. V gives a conclusion and an outlook to future work.

## II. GOVERNING EQUATIONS OF MULTICOMPONENT ELECTRO-HYDRODYNAMICS

In this section we are concerned with the equations of motion for a mixture composed of $N$ distinct ionic species in the regime of vanishing Mach number, influenced by external electric and gravitational fields, $\mathbf{E}$ and $\mathbf{g}$, respectively. Its mass balance for species $k$ in terms of its the molar concentration $n_k$ is given by

$$\partial_t n_k + \nabla \cdot (n_k \mathbf{w}) = -\nabla \cdot \mathbf{J}_k. \tag{1}$$

The molar and density averaged mixture velocities are defined by

$$\mathbf{w} = \sum_k \frac{n_k}{n}\mathbf{v}_k, \quad \mathbf{v} = \sum_k \frac{\rho_k}{\rho}\mathbf{v}_k. \tag{2}$$

Additionally, we define the mixture molar weight and number density fractions by

$$m = \frac{1}{n}\sum_k n_k m_k, \quad \chi_k = \frac{n_k}{n},$$

with $m_k$ the molar mass of species $k$, and find the following relation between molar fraction $\chi_k$ and mass density $\rho_k$: $\chi_k = \frac{m}{m_k}\frac{\rho_k}{\rho}$. The mixture's momentum conservation is given in terms of an incompressible Navier-Stokes equation with external forcing term

$$\partial_t \rho\mathbf{v} + \nabla \cdot (\rho\mathbf{v} \otimes \mathbf{v} + p\mathbf{I}) = \nu\nabla^2(\rho\mathbf{v}) + \underbrace{\rho\mathbf{g} + \rho^e\mathbf{E}}_{=:\mathbf{F}}. \tag{3}$$

Here $\mathbf{F}$ denotes the total mixture force per unit volume. The equations of motion are well posed when an additional closure relation for the diffusive fluxes $\mathbf{J}_k$ is provided.

It has been shown by experiments that the analytic predictions of an extended Maxwell-Stefan closure relation leads to reasonable results in case of electrolytes and electrodialytic processes ([30,31]). In our case, we consider the following extended Maxwell-Stefan model ([32,33]) (where $\mathcal{F}$ denotes the Faraday constant, $\mathbf{E}$ the electric field, $z_k$ the ionic charge of species $k$, $V_k$ its molar volume, and $y_k = \rho_k/\rho$ its mass fraction):

$$\left(\sum_i \Gamma_{k,i}\nabla\chi_i\right) - \mathbf{F}_k + \frac{n_k V_k - y_k}{nRT}\nabla p = \sum_{l\neq k}\frac{1}{D_{k,l}n}(\chi_k\mathbf{J}_l - \chi_l\mathbf{J}_k), \tag{4}$$

where the external diffusive forcing term $\mathbf{F}_k$ for species $k$ is defined by

$$\mathbf{F}_k = \frac{1}{nRT}\rho_k\left(\mathbf{g} + \frac{z_k\mathcal{F}}{m_k}\mathbf{E}\right) - \frac{y_k}{nRT}\sum_{l=1}^{N}\rho_l\left(\mathbf{g} + \frac{z_l\mathcal{F}}{m_l}\mathbf{E}\right). \tag{5}$$

Please notice that, by definition of $\mathbf{F}_k$, the sum of the external diffusive forces vanishes. Furthermore, we notice that the diffusive forcing terms related to the gravitation acceleration in $\mathbf{F}_k$ cancel out. Additionally, in case of an electroneutral mixture (zero charge of the mixture), we have

$$\rho^e = \sum_{l=1}^{N}\mathcal{F}\frac{\rho_l z_l}{m_l} = \sum_{l=1}^{N}\mathcal{F}n_l z_l = 0,$$

thus the electric forcing term in the summation part of $\mathbf{F}_k$ vanishes. In general, the external diffusive forces $\mathbf{F}_k$ can be decomposed into two parts: The total external force for species $k$ [i.e., $\rho_k(\mathbf{g} + \mathbf{E}z_k\mathcal{F}/m_k)/(nRT)$] and the fraction of the total mixture force acting on the species $k$ [i.e., $y_k(\sum_l \rho_l(\mathbf{g} + \mathbf{E}z_l\mathcal{F}/m_l))/(nRT)$]. By subtracting these two parts, $\mathbf{F}_k$ contains only that part of the external forces acting exclusively on species $k$. The total mixture force is added to the momentum equation that leads to a transport of all species by advection of the mixture [cf. Eq. (3)].

The binary Maxwell-Stefan diffusivities in (4) can be calculated in an electroneutral electrolyte solution by [27,34]

$$D_{i,j} = \tilde{D}_1(i,j) + \tilde{D}_2(i,j)n_{i+j} + \tilde{D}_3(i,j)n_{i+j}^{3/2} + \tilde{D}_4(i,j)n_{i+j}^2 + \tilde{D}_5(i,j)\sqrt{n_{i+j}}, \tag{6}$$

where $\tilde{D}_1(i,j), \ldots, \tilde{D}_5(i,j)$ are species-dependent coefficients and $n_{i+j} = n_i + n_j$ denotes the combined number density of species $i$ and $j$. For nonelectroneutral conditions we use properly adapted rules for binary Maxwell-Stefan diffusivities, as given in Ref. [34], and we refer the reader to this publication for a detailed discussion. Appendices A1 and A2 provide numerical values for aqueous NaCl and $H_2SO_4$ solutions. It is worth pointing out that even in simple electrolytes, e.g., aqueous NaCl mixture, diffusivities show a significant dependence on ionic concentrations in the liquid, as $\tilde{D}_1(\mathrm{Na,Cl}) = 0$. Furthermore, it is easy to check that, according to Eq. (6), Maxwell-Stefan diffusivities themselves might be negative. Although this seems to be wrong intuitively, it is sufficient to ensure a positive-definite condition of the Maxwell-Stefan diffusivity matrix to ensure well-posedness. A detailed investigation is given in Ref. [35] and we refer to it in Sec. IV A, Eq. (14).

The left-hand side of Eq. (4) is coupled by a matrix $\Gamma$ that contains the thermodynamic factors [26]. The thermodynamic factor matrix is related to the concept of activity coefficients $\gamma_k$ and for electrolytes its functional dependence is given by [36]

$$\Gamma_{k,i}(\mathbf{x},t) = \delta_{k,i} + \chi_k(\mathbf{x},t)\frac{\partial \ln\gamma_k}{\partial\chi_i}|_{(\mathbf{x},t)}.$$

A short derivation of the thermodynamic factors from thermodynamic principles is given in Appendix B. From the physical point of view, activity coefficients take into account

the deviations from ideal behavior in a multicomponent fluid in the following sense: In an ideal mixture, any interaction between two species is the same, hence properties of the mixture may be expressed directly in terms of species' concentrations or partial pressures. However, in nonideal mixtures, as electrolytes, these concentrations have to be scaled properly by activity coefficients. Even at very low concentrations electrolytes show a significant deviation from ideal behavior, an effect that has been known for a long time [25], and thus activity coefficients play an important role in mathematical models of such mixtures. A number of different models for the evaluation of activity coefficients and thermodynamic factors exist. Theoretical activity coefficient models include the Debye-Hückel model [25] and its extensions, e.g., Davies [37], Pitzer [38], and TCPC [39]. For concentrated electrolyte solutions, activity coefficients can also be evaluated by use of correlative methods, e.g., MOSCED, (e)NRTL, UNIQUAC, and UNIFAC. We refer the reader to Ref. [36] for a complete overview of these models. It should be noted that all of these models are consistent with the Maxwell-Stefan formulation without thermodynamic factors in the limit of vanishing concentrations, i.e., $\gamma_k \to 1$ when $\chi_k \to 0$ or $\chi_k \to 1$.

The electric potential $\psi$ (and hence the electric field $E = -\nabla\psi$) are obtained by

$$-\Delta\psi = \frac{\mathcal{F}}{\epsilon^{\text{mix}}} \sum_{k=1}^{N} n_k z_k. \tag{7}$$

In combination with properly defined boundary conditions (Neumann or Dirichlet) the upper equation provides a well-posed potential equation for the electric potential, where $\epsilon^{\text{mix}}$ denotes mixture's permittivity.

## III. A SIMPLIFIED KINETIC MODEL FOR MULTICOMPONENT ELECTRO-HYDRODYNAMICS

In this section we present a simplified kinetic model, a finite discrete velocity model (FDVM), consistent with the electrolyte's equation of motion. It recovers them in the asymptotic limit of vanishing Knudsen and Mach number. Additionally, this FDV model will be the starting point for our lattice Boltzmann model (LBM) that will be derived by spatial and temporal discretization in Sec. IV.

In the BGK-FDV model we restrict the full Boltzmann equation to a finite set of $M$ discrete velocities and replace the collision operator with its BGK version [40] (where $m \in \{0, \dots M-1\}$) as follows:

$$\partial_t f_k^m + \mathbf{u}^m \cdot \nabla f_k^m = \underbrace{\lambda_k \left(f_k^{\text{eq},m} - f_k^m\right)}_{=:\mathcal{C}_k^m(f)} + d_k^m. \tag{8}$$

The collision parameter $\lambda_k$ is defined by $\lambda_k = BK/p'$, where $B$ denotes a collision frequency, $p'$ denotes an upper limit of the mixture pressure variations, and $K$ denotes the bulk modulus of the liquid mixture measuring the mixture's resistance to uniform compression. Numerical values for some electrolytes relevant in electrodialysis can be found, for example, in Ref. [41]. In particular, we obtain $c_s^2 = K/\rho$ and, for later use, we define the ratio of background density to pressure fluctuations by $\mathcal{C} = B\rho/p'$. Obviously, we assign the same relaxation parameter to all the species in our model. As already shown in Ref. [20], this does not restrict us to a single independent diffusion parameter, as momentum exchange among the species is modeled by $\rho_k \mathbf{v}_k^*$ in $f_k^{\text{eq},m}$, cf. (9). The forcing term $d_k^m$ is directly related to the diffusive driving forces and mixture forces in (4) and (3). In the FDV model density and momentum can be obtained by

$$\rho_k = \sum_{m=0}^{M-1} f_k^m, \quad \mathbf{j}_k = \sum_{m=0}^{M-1} \mathbf{u}^m f_k^m.$$

The right-hand side of Eq. (8) is the collision operator of the BGK model and relaxes the species probability density function $f_k^m$ towards its thermodynamic equilibrium with a given relaxation parameter $\lambda_k$ to achieve the desired macroscopic behavior. We define

$$\rho_k \mathbf{v}_k^* = \left[ \rho_k \mathbf{v}_k + \sum_l \Gamma_{k,l}^{-1} \rho_l \sum_\zeta \chi_\zeta \frac{B_{l,\zeta}}{\mathcal{C}} \phi_l (\mathbf{v}_\zeta - \mathbf{v}_l) \right], \tag{9}$$

where $B_{k,l} = 1/D_{k,l}$ are Maxwell-Stefan resistivities and set the thermodynamic equilibrium as follows (where $k$ is the species index):

$$f_k^{\text{eq},m} = \omega_m \left[ \rho_k s_m^k + \frac{1}{c_s^2} (\mathbf{u}^m \cdot \rho_k \mathbf{v}_k^*) + \frac{\rho_k}{2c_s^4} (\mathbf{u}^m \cdot \mathbf{v})^2 - \frac{\rho_k}{2c_s^2} \mathbf{v}^2 \right]. \tag{10}$$

The modifications, compared to Refs. [20,22], are twofold: First, we make use of a modified velocity in the bilinear part of the collisions. This allows us to recover thermodynamic factors in the Maxwell-Stefan equations. In contrast to Ref. [20], in our model $\sum_k \rho_k \mathbf{v}_k^* \neq \sum_k \rho_k \mathbf{v}_k$ due to the inclusion of the thermodynamic factors. In Sec. III A, we show that a slightly generalized condition holds true [cf. Eqs. (12) and (13)]. Second, we replace the velocities in the quadratic equilibrium part with the mixture-averaged velocities. Hereby we recover the correct mixture Navier-Stokes equation even in regimes where the mixture-averaged diffusion approximation does not hold. In addition, we choose $s_0^k = \frac{1}{\omega_0} + (1 - \frac{1}{\omega_0})\phi_k$, $s_{m\neq 0}^k = \phi_k$. The coefficient $\phi_k$ defines the equation of state in our FDV model, i.e., $p_k = c_s^2 \phi_k \rho_k$. In general, any equation of state is possible in our model, but two restrictions have to be considered: The equation of state should depend on the slow mass diffusion time scales and its corresponding quantities solely, e.g., $\rho_k^{(0)}$ cf. Sec. III B. From the numerical point of view it should be bounded by 1 to guarantee stability of the model. In the following we set $\phi_k = \min_\alpha m_\alpha / m_k \leqslant 1$. The weights $\omega_m$ are chosen to guarantee lattice isotropy conditions, e.g., as defined for the D2Q9, D3Q15, or D3Q19 lattice [29].

It is worth emphasizing that the upper model satisfies the indifferentiability whenever the activity coefficient model satisfies $\gamma_k \to 1$ for $\chi_k \to 0$ and $\chi_k \to 1$.

### A. Diffusive driving forces and collision invariants

Similarly to the decomposition of the external forces into diffusive driving forces (slow mass diffusion time scale, cf. Sec. II) and mixture forces (fast viscous time scale), we split the mesoscopic forcing term in (8) into $d_k^{m,1}$ and $d_k^{m,3}$,

respectively. We relate the forcing term in the FDVM to (5) by

$$d_k^m = \underbrace{\min_\alpha m_\alpha \omega_m \mathbf{u}_m \cdot \sum_l \Gamma_{k,l}^{-1} n \left( \mathbf{F}_l - \frac{n_l V_l - y_l}{nRT} \nabla p \right)}_{=:d_k^{m,(1)}\text{(diff. driv. forces)}} + \underbrace{\frac{\omega_m}{c_s^2} \mathbf{u}_m \cdot (\rho_k \mathbf{g} + \mathcal{F} n_k z_k \mathbf{E})}_{=:d_k^{m,(3)}\text{species' mix. force fraction}}. \quad (11)$$

The mixture pressure gradient $\nabla p$ can be obtained by a centered finite difference with second-order accuracy on the compact lattice Boltzmann stencil. Of course, this finite difference correction is not necessary whenever $\Gamma_{i,j} = \delta_{i,j}$, cf. Ref. [42].

It should be noted that most activity models do not provide a formal dependency of the pressure and therefore the partial molar volume $V_k = \partial^2 g/(\partial n_i \partial p)$ cannot be obtained ($g$ denotes the molar Gibbs free energy). This is due to the fact that, in practice, correlation-based activity models would require a large amount of parameters. Hence, additional density models for electrolytes have been developed and applied. A detailed discussion and our density model of choice is given in Ref. [43]. Besides this technical discussion, the upper density model fixes the equation of state, as it provides a formal dependency $V_k = f(n_1, \ldots, n_N, p, T)$.

Compared to the previous work in Ref. [22], no correction term for the stress tensor in the presence of external forcing $\mathbf{F}_k$ is necessary in Eq. (11) (even in the case where $\mathbf{F}_k$ and $\mathbf{F}$ are nonzero) due to the fact that the spurious terms cancel out by construction. Therefore, derivatives of the forcing terms are unnecessary. This can be easily checked by considering the asymptotic limit of the FDVM.

Although it has been shown in Ref. [20] that $\mathbf{j}_k \neq \sum_m \mathbf{u}^m f_k^{\text{eq},m}$, we can furthermore check that in our model

$$\sum_m \mathcal{C}_k^m(f) = 0, \quad \sum_m d_k^{m,(1)} = 0 \quad (12)$$

and

$$\sum_{k,m} \mathbf{u}^m \left[ \mathcal{C}_k^m(f) + d_k^{m,(1)} \right] = 0 \quad (13)$$

are satisfied. These three relations guarantee that each species' mass, as well as mixture momentum (up to third order), are collision invariants of our FDV model. In general, the latter holds true only whenever external diffusive driving forces are properly considered [as done in (13)]. While (12) is obvious (cf. Ref. [20]), it is worth pointing out that (13) is naturally true, as the presented FDV model recovers the Maxwell-Stefan formulation (including thermodynamic factors and external driving forces). This can be seen very easily by considering Eq. (4) in matrix-vector notation as follows:

$$\Gamma \begin{pmatrix} \nabla \chi_1 \\ \vdots \\ \nabla \chi_N \end{pmatrix} - \begin{pmatrix} \mathbf{F}_1 \\ \vdots \\ \mathbf{F}_N \end{pmatrix} = \begin{bmatrix} \sum_{\zeta \neq 1} \frac{B_{1,\zeta}}{n} (\chi_1 \mathbf{J}_\zeta - \chi_\zeta \mathbf{J}_1) - \frac{n_1 V_1 - y_1}{nRT} \nabla p \\ \vdots \\ \sum_{\zeta \neq N} \frac{B_{N,\zeta}}{n} (\chi_N \mathbf{J}_\zeta - \chi_\zeta \mathbf{J}_N) - \frac{n_N V_N - y_N}{nRT} \nabla p \end{bmatrix}.$$

Inverting the matrix $\Gamma$ and summation of corresponding rows leads to

$$\sum_k \nabla \chi_k = \sum_k \sum_l \Gamma_{k,l}^{-1} \left[ \sum_\zeta \frac{B_{l,\zeta}}{n} (\chi_l \mathbf{J}_\zeta - \chi_\zeta \mathbf{J}_l) + \mathbf{F}_l - \frac{n_l V_l - y_l}{nRT} \nabla p \right].$$

Taking advantage of $\sum_k \chi_k = 1$ and $\mathbf{J}_i = n_i(\mathbf{v}_i - \mathbf{w})$ we get

$$0 = \sum_k \sum_l \Gamma_{k,l}^{-1} \left[ \sum_\zeta \frac{B_{l,\zeta}}{n} \chi_l \chi_\zeta (\mathbf{v}_\zeta - \mathbf{v}_l) + \mathbf{F}_l - \frac{n_l V_l - y_l}{nRT} \nabla p \right],$$

which is equivalent to (13). Physically, the upper technical discussion proves that the presented FDVM ensures vanishing total diffusive driving forces (no matter whether the driving forces are internal or external).

### B. The asymptotic limit of vanishing Mach and Knudsen number

The presented mesoscopic FDV method of the previous section recovers the electro-hydrodynamic equations of Sec. II asymptotically, in the limit of small Knudsen and Mach number, with second order in space and first order in time. This can be shown rigorously by considering the diffusive asymptotic limit [28], i.e., scaling as $\widetilde{\Delta x} = \epsilon \Delta x$, $\widetilde{\Delta t} = \epsilon^2 \Delta t$. Much effort has been spent over the past several years to analyze LBM-like schemes rigorously and we refer the reader to Ref. [29] and to the previous work in Refs. [20,22,42] for mixture models based on the work of Ref. [23]. In the following we provide only the key concepts to connect (8) to (1), (4), (5), and (3) and point out the differences to the mentioned publications. We adopt the notation of Ref. [20] in the following. The diffusive asymptotic limit is usually considered for analyzing continuum low Mach limit in Hilbert expansions [28] and provides a direct mathematical relation between the Boltzmann equation and the incompressible Navier-Stokes equation. However, alternative scalings, as well as expansions, are possible [44] and therefore the following analysis serves as a mathematical example in the low Mach and continuum limit.

Considering the diffusive mass transport in the proposed FDV model, cf. Eqs. (47) and (49) in Ref. [20], we obtain

$$\nabla \rho_k^{(0)} = \sum_{m=1}^{M} \frac{\mathbf{u}_m d_k^{m,(1)}}{\phi_k c_s^2} + \frac{\lambda_k}{\phi_k c_s^2} \sum_{\substack{j,l \geqslant 0 \\ j+l=1}} \left(\rho_k^{(j)} \mathbf{v}_k^{(l)}\right)^* - \rho_k^{(j)} \mathbf{v}_k^{(l)}.$$

After some algebra and inversion of the thermodynamic factor matrix, it can be shown that this equation ensures that (1) and (4) are satisfied. By construction of $\rho_k \mathbf{v}_k^*$ and $d_k^{m,1}$ the recovered Maxwell-Stefan formulation includes thermodynamic factors $\Gamma$ and diffusive driving forces $\mathbf{F}_k$. Furthermore, it should be noted that the calculation of the Maxwell-Stefan diffusivities, according to (6), and the thermodynamic factors, is solely based on the slow scales and corresponding quantities, e.g., $n_k^{(0)}$. Overall, we recover for the diffusive mass transport

$$\left[\sum_i \Gamma_{k,i} \nabla \chi_i^{(0)}\right] - \mathbf{F}_k + \frac{n_k^{(0)} V_k - y_k^{(0)}}{n^{(0)} RT} \nabla p = \sum_{l \neq k} \frac{1}{D_{k,l} n^{(0)}} \left[\chi_k^{(0)} \mathbf{J}_l^{(1)} - \chi_l^{(0)} \mathbf{J}_k^{(1)}\right].$$

It is worth emphasizing that the barodiffusion term in $d_k^m$, obtained by use of a centered finite difference, is usually small in the diffusive asymptotic limit.

Regarding the mixture momentum transport the following observations can be made: In comparison to Eq. (54) in Ref. [20] we obtain a slightly different momentum flux tensor for each species. When summing over the species index $k$, the result is a correct nonlinearity of the mixture Navier-Stokes equation,

$$\sum_{k,m} \mathbf{u}_m \otimes \mathbf{u}_m f_k^{m,(2)} = c_s^2 \sum_k \phi_k \rho_k^{(2)} \mathbf{I} + \rho^{(0)} \mathbf{v}^{(1)} \otimes \mathbf{v}^{(1)} + \frac{1}{\mathcal{C}} [\nabla \rho^{(0)} \mathbf{v}^{(1)} + (\nabla \rho^{(0)} \mathbf{v}^{(1)})^T].$$

Thus, we recover the correct hydrodynamic behavior of the electrolyte solution [i.e., (3) with $\nu = 1/\mathcal{C}$], even when the diffusive fluxes are large and the mixture averaged diffusion approximation is not satisfied.

Independent of the asymptotic scaling under consideration, a few general remarks with respect to the external forcing terms can be given. By formally expanding the forcing term $d_k^m = \sum_{i \geqslant 0} \epsilon^i d_k^{m,(i)}$, different orders of forcing become apparent. Diffusive driving forces are large, appearing on $d_k^{m,1}$ scales, while mixture forces are small (i.e., $d_k^{m,(3)}$ in case of diffusive asymptotic limit). However, it is important to ensure that $\sum_k \sum_m \mathbf{u}_m (\mathcal{C}_k^m(f) + d_k^{m,(i)}) = 0$ (for $i \leqslant 2$ for diffusive asymptotic analysis) to guarantee consistency to the low-Mach assumption). It is worth emphasizing that (11) guarantees this by construction for the diffusive asymptotic limit (to the knowledge of the authors this question has not been addressed rigorously so far, cf. discussion below (39) in Ref. [22]). Our model ensures this condition in the diffusive limit even when the mixture is not electroneutral and in the presence of strong electric driving forces, a situation that is likely to occur in boundary layers of electrodialysis processes, the so-called diffusive double layer [33]. In fact, the correct coverage of this phenomena is mandatory to study strongly nonlinear effects as electroconvective vortices [45,46].

## IV. NUMERICAL EXPERIMENTS

To derive a fully discrete model, we integrate the FDVM along its characteristics [47,48]. While the left-hand side of (8) is integrated analytically, the particular fully discrete model is obtained by choosing a specific approximation for the integral of the collision term. We choose a trapezoidal rule for stability and accuracy [20]. After applying a reformulation in terms of the transformed variable $\bar{f}_k^m = f_k^m + \frac{\delta t \lambda_k}{2}(f_k^m - f_k^{\mathrm{eq},m})$, an explicit Lattice Boltzmann scheme is obtained,

$$\bar{f}_k^m(\mathbf{x} + \mathbf{u}^m \delta t, t + \delta t) - \bar{f}_k^m(\mathbf{x}, t) = \frac{\delta t}{\frac{1}{\lambda_k} + \frac{\delta t}{2}} \left[f_k^{\mathrm{eq},m}(\mathbf{x}, t) - \bar{f}_k^m(\mathbf{x}, t)\right] + d_k^m(\mathbf{x}, t).$$

A few remarks on the upper discrete algorithm can be made. After each time step the electric potential equation (7) is solved numerically to compute the external driving forces; density distributions are used to evaluate activities, diffusivities, and the finite difference correction for the barodiffusion term. To complete the assembly of the right-hand side of the upper discrete scheme, we solve an elemental linear equation system to recover the correct momentum $\mathbf{j}_k$ from the transformed variables,

$$\begin{aligned}\bar{\mathbf{j}}_k &= \langle 1, \mathbf{u}^m \bar{f}_k^m \rangle = \mathbf{j}_k + \frac{\delta t \lambda_k}{2} \left(\mathbf{j}_k - \langle 1, \mathbf{u}^m f_k^{\mathrm{eq},m} \rangle\right) \\ &= \mathbf{j}_k - \frac{\delta t \lambda_k}{2} \sum_\zeta \mathbf{j}_\zeta \sum_l \Gamma_{k,l}^{-1} \frac{B_{l,\zeta}}{\mathcal{C}} \phi_\zeta \chi_l \\ &\quad + \frac{\delta t \lambda_k}{2} \sum_l \mathbf{j}_l \sum_\zeta \Gamma_{k,l}^{-1} \frac{B_{l,\zeta}}{\mathcal{C}} \chi_\zeta \phi_l.\end{aligned}$$

After these steps, collision and streaming can be carried out to complete the time step. In contrast to the implementation described in Ref. [20], the presented method considers variable

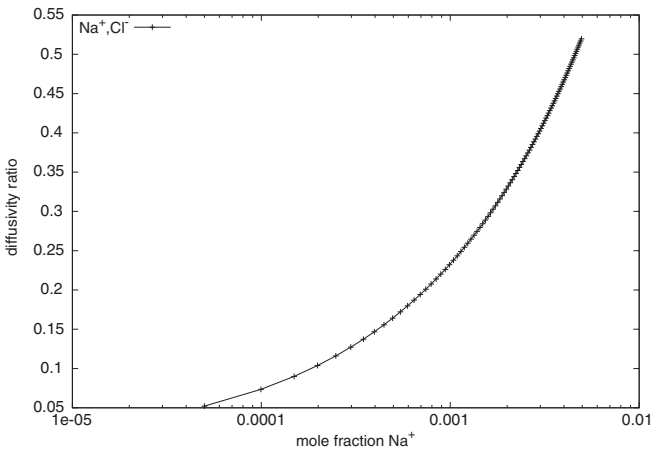


FIG. 1. Ratio of nonideal (i.e., concentration dependent) and ideal (i.e., constant) Maxwell-Stefan diffusivity for $Na^+$,$Cl^-$ as function of $Na^+$ mole fractions in an electroneutral mixture of $H_2O$,$Na^+$,$Cl^-$, according to model (6) and the parameters of Table I.

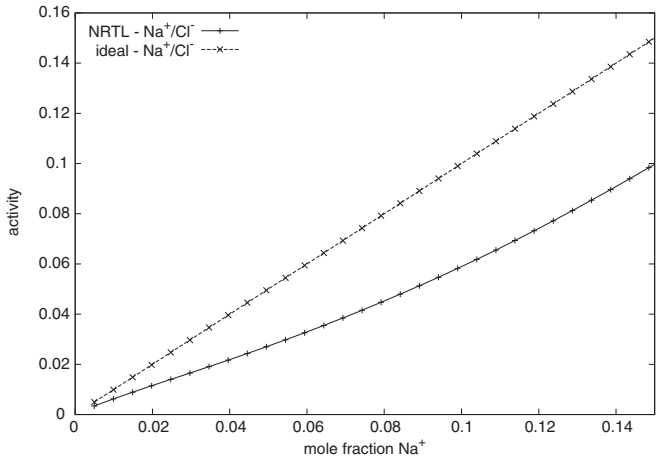


FIG. 2. Activity of $Na^+/Cl^-$ as function of $Na^+$ mole fractions in an electroneutral mixture of $H_2O$,$Na^+$,$Cl^-$ (predicted by the NRTL model).

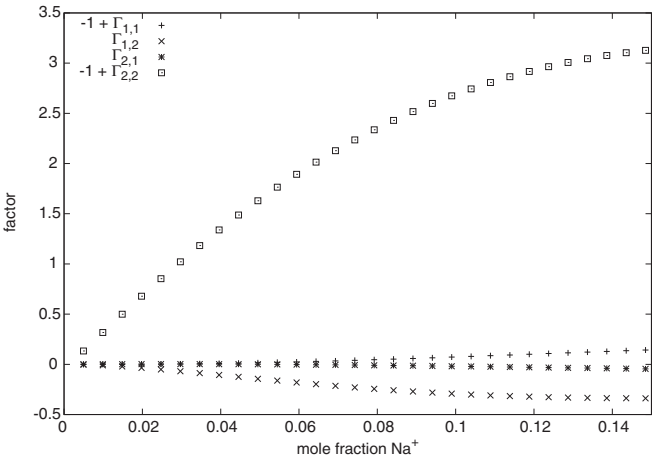


FIG. 3. Deviation of thermodynamic factors from ideal behavior as function of $Na^+$ mole fractions in an electroneutral mixture of $H_2O$,$Na^+$,$Cl^-$ (predicted by an NRTL model). In an ideal mixture all lines would equal zero. Due to symmetry only the relevant entries of $\Gamma$ are shown.

diffusivities and thermodynamic factors and, hence, the elemental variable system changes in each iteration. Therefore, no precomputation of the inverse can be done. In the course of our numerical experiments in Secs. IV A and IV B, the elemental linear equation system has been well posed in every time step.

The presented lattice Boltzmann scheme is coupled to a nodal, first-order finite element method (FEM) [49] to solve the electric potential equation on the same domain as the lattice Boltzmann method. The coupling is achieved by a simple first-order accurate interpolation in both directions [from vertex- (FEM) to barycentric- (LBM) based values and vice versa]. Both meshes have similar spatial resolutions. Due to the simplicity of the presented lattice Boltzmann method, most of the time is spent solving the electric potential equation by use of the FEM.

### A. Thin diffusive double layer for $H_2O$-NaCl

We consider a mixture of NaCl and $H_2O$. The deviation of the Maxwell-Stefan diffusivities, activity coefficients, and thermodynamic factors from ideal Maxwell-Stefan coefficients as a function of $Na^+$ mole fractions are given in Figs. 1, 2, and 3, respectively. The Maxwell-Stefan diffusivities have been computed according to model (6) and the parameters are shown in Table I. According to the given diffusivity model, it is obvious that for low concentrations the Maxwell-Stefan diffusivities of $D_{Na^+,Cl^-}$ might become negative. The effect is well known and has been discussed many times, e.g., Ref. [35]. The authors point out that the only relevant restriction on the diffusivities arises from the fact that the overall entropy production has to be positive (including all driving forces) and this can be ensured whenever

$$0 \leqslant \left(\sum_{i\neq k} \frac{\chi_i \chi_k}{D_{i,k}}\right)\left(\sum_{j\neq l} \frac{\chi_j \chi_l}{D_{j,l}}\right) - \left(\frac{\chi_k \chi_l}{D_{k,l}}\right)^2 \qquad (14)$$

holds true for all $k$ and all $l$ with $k \neq l$. Essentially, the upper equation is a constraint on the positive definiteness of the diffusivity matrix and can be satisfied even for negative Maxwell-Stefan diffusivities [35]. In our simulations Eq. (14) has always been satisfied. The geometrical setup is a simple microchannel of length $L$ in the $x$ direction (periodic in the $y$ direction), homogeneously filled with a mixture of $H_2O$,$Na^+$,$Cl^-$, initially. We denote the initial values by $\chi^0_{H_2O}, \chi^0_{Na^+}, \chi^0_{Cl^-}$ in the following.

To create a nonelectroneutral, thin diffusive double layer, we apply a drop in the electric potential by imposing Dirichlet boundary conditions,

$$\psi(0,t) = V_0, \quad \psi(L,t) = 0.$$

Initially, the electrical, external driving force moves oppositely charged species into opposite directions and creates nonelectroneutral regimes. The process continues until driving forces that result from gradients in chemical and electrical potentials equilibrate; a thin nonelectroneutral layer at the boundaries, the so-called diffusive double layer, is formed.

At first we consider low electrolyte concentrations. In this regime nonideal effects are small and we can compare the coupled simulation results to existing, leading-order analytical predictions [50–52]. The resulting concentration profiles for

TABLE I. Parameter values $\tilde{D}_1(i,j), \ldots, \tilde{D}_5(i,j)$ (given as multiples of $10^{-9}$) for a liquid NaCl solution as reported in Ref. [34].

| $(i,j)$ | $\tilde{D}_1$ | $\tilde{D}_2$ | $\tilde{D}_3$ | $\tilde{D}_4$ | $\tilde{D}_5$ |
|---|---|---|---|---|---|
| Na,Cl | 0 | $8.02 \times 10^{-5}$ | $-2.09 \times 10^{-7}$ | $-7.03 \times 10^{-9}$ | $2.18 \times 10^{-3}$ |
| Na,$H_2O$ | 1.34 | $-3.06 \times 10^{-5}$ | $-3.91 \times 10^{-6}$ | $3.77 \times 10^{-8}$ | $-1.77 \times 10^{-3}$ |
| Cl,$H_2O$ | 2.04 | $-2.24 \times 10^{-4}$ | $-3.79 \times 10^{-6}$ | $3.78 \times 10^{-8}$ | $8.32 \times 10^{-3}$ |

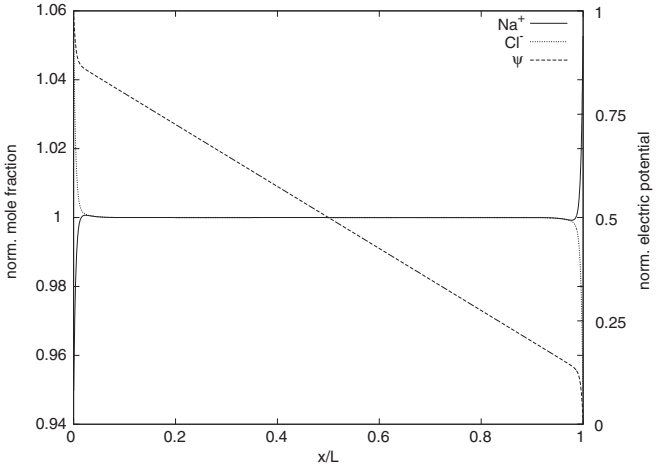


FIG. 4. Normalized mole fraction and electric potential profiles for $Na^+$ and $Cl^-$ in the $\mu$ channel.

$Na^+$ and $Cl^-$ are shown in Fig. 4. Figure 5 shows a close-up of the nonelectroneutral region. The thin double layer is clearly visible close to the boundary. Around the center region, where concentration gradients are very small, the mixture is electroneutral, due to the strong electrostatic interactions among the species. In the leading order approximation, the concentration profile of the ionic species in the double-layer region is given by $\chi_i(x) = C_i^1 \exp(C_i^2 x) + \chi_i^0$ (where $C_i^2 < 0$ and the sign of $C_i^1$ is determined by the charge of the species $i$). For the electric potential in the double-layer region we obtain in leading order $\psi(x) = C_1^\psi \exp(C_2^\psi x) + C_3^\psi x + C_4^\psi$. For a detailed analysis, we refer the reader to Refs. [50–52]. Overall, the coupled lattice Boltzmann–finite element simulation results are close to the leading order predictions (cf. Fig. 5).

Figure 6 shows a comparison of simulations at high electrolyte concentrations, where nonideal effects are important, among different lattice Boltzmann models: The presented model, the presented model without the finite difference correction for the barodiffusion term, and the model in Ref. [20],

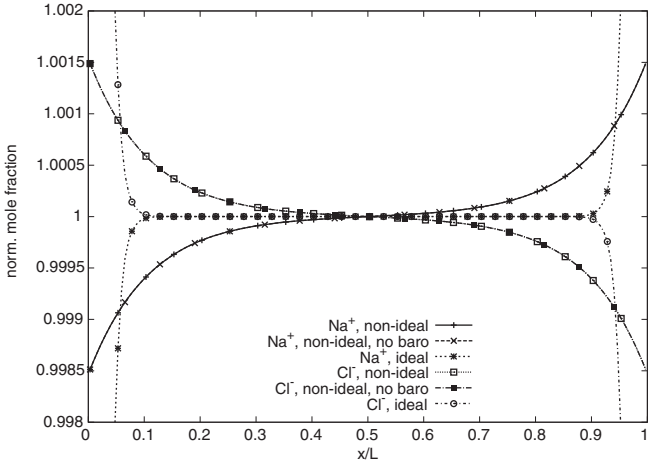


FIG. 6. Comparison of double-layer concentration profiles for various lattice Boltzmann models: "nonideal" refers to the presented model, "nonideal, no-baro" to the presented model without finite difference correction for the barodiffusion, and "ideal" to the model presented in Ref. [20].

suited for ideal gas phases. Obviously, the presented model leads to much larger boundary layers than the model suited for ideal gas phases due to the following fact: Thermodynamic factors weight the driving forces $\nabla\chi_i$ in the Maxwell-Stefan formulation [cf. Fig. 3 and Eq. (4)]. As the potential drop across the channel is prescribed, the main driving forces of the system, i.e., chemical and electrical driving forces, equilibrate at smaller concentration gradients with a larger double-layer size.

### B. Large molecular-weight ratio ($H_2O$-$H_2SO_4$)

In this section we consider a setup similar to that in the previous section but test our model with a high-molecular-weight ratio of $m_{SO_4^{2-}}/m_{H^+} > 95$. The corresponding Maxwell-Stefan diffusion coefficients are calculated by use of the coefficients from Table II. Furthermore, an adapted eNRTL model for $H_2O - H_2SO_4$ has been applied. A close-up of the resulting

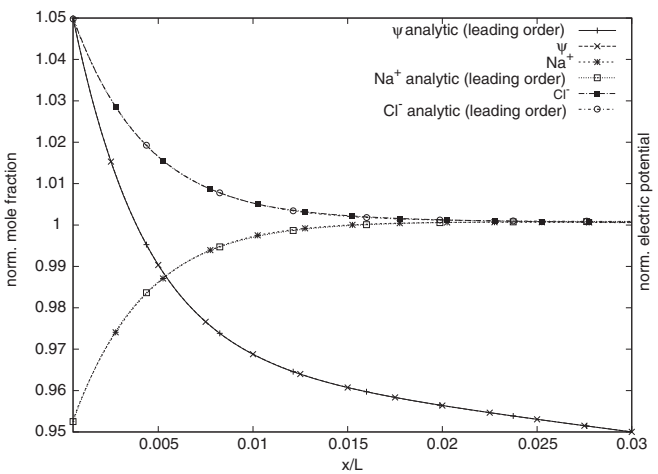


FIG. 5. Close-up of normalized mole fraction and electric potential profiles for $Na^+$ and $Cl^-$ in the $\mu$ channel.

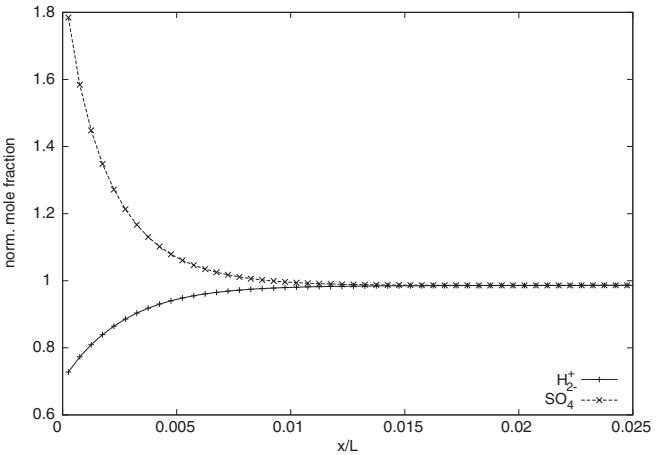


FIG. 7. Close-up of normalized mole fraction profiles for $H^+$ and $SO_4^{2-}$ in the double-layer region of the $\mu$ channel.

TABLE II. Parameter values $\tilde{D}_1(i,j), \ldots, \tilde{D}_5(i,j)$ (given as multiples of $10^{-9}$) for a liquid $H_2SO_4$ solution as reported in Ref. [34].

| $(i,j)$ | $\tilde{D}_1$ | $\tilde{D}_2$ | $\tilde{D}_3$ | $\tilde{D}_4$ | $\tilde{D}_5$ |
|---|---|---|---|---|---|
| $H,SO_4$ | 0 | $2.545 \times 10^{-4}$ | $-9.089 \times 10^{-7}$ | $-2.240 \times 10^{-8}$ | 0.0 |
| $H,H_2O$ | 9.313 | $-1.431 \times 10^{-2}$ | $2.197 \times 10^{-4}$ | $-1.148 \times 10^{-6}$ | $2.176 \times 10^{-1}$ |
| $SO_4,H_2O$ | 1.068 | $-9.998 \times 10^{-4}$ | $1.437 \times 10^{-5}$ | $-7.335 \times 10^{-8}$ | $1.525 \times 10^{-2}$ |

concentration profiles for $H^+$ and $SO_4^{2-}$ is shown in Fig. 7. The double layer is well resolved.

## V. CONCLUSION AND FUTURE WORK

In this paper we presented a new finite discrete velocity model for electrolytes. It recovers mass conservation, the incompressible Navier-Stokes equation, and the Maxwell-Stefan equations. The building blocks of the extension to electrolytes are the rigorous coverage of external driving forces, the inclusion of thermodynamic factors for nonideal diffusion, and concentration-dependent diffusivities. A fully discrete lattice Boltzmann scheme is derived by integration along the characteristics. Numerical experiments show the validity of the presented model for electrolyte solutions.

## ACKNOWLEDGMENTS

This work was funded by the German Federal Ministry of Education and Research (Bundesministerium für Bildung und Forschung, BMBF) in the framework of the HPC software initiative in the project HISEEM. P.A. acknowledges the support of the Italian Ministry of Research (FIRB Grant No. RBFR10VZUG).

## APPENDIX A: MAXWELL-STEFAN DIFFUSIVITIES FOR ELECTROLYTE SOLUTIONS

The concentration-dependent Maxwell-Stefan diffusion coefficients for a liquid NaCl and $H_2SO_4$ solution have been estimated in Ref. [34] using Eq. (6). The results are obtained by experimental data from Ref. [27]. Parameter values for $\tilde{D}_{i,j}$ are summarized in Table I and Table II, respectively.

### 1. Liquid NaCl solution

The correlation (6) can be applied for a NaCl concentration range of 0–5000 $\mathrm{mol/m^3}$.

### 2. Liquid $H_2SO_4$ solution

The correlation (6) can be applied for a $H_2SO_4$ concentration range of 0–6000 $\mathrm{mol/m^3}$.

## APPENDIX B: THERMODYNAMIC FACTORS IN THE MAXWELL-STEFAN FORMULATION

In the following we briefly review the derivation of the formal shape of Eq. (4) from irreversible thermodynamics. A detailed version can be found in Ref. [32]. The diffusive driving forces $\mathbf{d}_k$ for species $k$ are related to the diffusive fluxes by

$$nRT\mathbf{d}_k = \sum_{l \neq k} \frac{RT}{D_{k,l}}(\chi_k \mathbf{J}_l - \chi_l \mathbf{J}_k).$$

The driving forces are proportional to gradients in the electro-mechanical-chemical potential

$$nRT\mathbf{d}_k = n_k \nabla \mu_k^{e,m,c} = n_k \nabla \mu_k - y_k \nabla p - \mathbf{F}_k.$$

The chemical potential of each species can be obtained by molar Gibbs free energy $g$ by $\mu_k = \partial g / \partial n_k$. In addition, the chemical potential is given by

$$\mu_k = \mu_0 + RT \ln a_k = \mu_0 + RT \ln \gamma_k n_k,$$

where $a_k$ is the species' activity and $\gamma_k$ is its activity coefficient. Hence

$$n_k \nabla \mu_k = nRT \sum_i \left( \delta_{k,i} + \chi_k \frac{\partial \ln \gamma_k}{\partial \chi_i} \right) \nabla \chi_i + n_k V_k \nabla p,$$

where we used $V_k = \partial \mu_k / \partial p$.

[1] S. Chen and G. D. Doolen, Annu. Rev. Fluid Mech. **30**, 329 (1998).
[2] J. Bernsdorf, U. Jaekel, T. Zeiser, T. Takei, H. Matsumoto, and K. Nishizawa, in *Computational Science* (Springer, Berlin, 2003), pp. 665–666.
[3] C. K. Aidun and J. R. Clausen, Annu. Rev. Fluid Mech. **42**, 439 (2010).
[4] S. Geller, M. Krafczyk, J. Tolke, S. Turek, and J. Hron, Comput. Fluids **35**, 888 (2006).
[5] S. Succi, *The Lattice Boltzmann Equation for Fluid Dynamics and Beyond*, Vol. 1 (Clarendon Press, London, 2001).
[6] V. Novaresio, M. García-Camprubí, S. Izquierdo, P. Asinari, and N. Fueyo, Comput. Phys. Commun. **183**, 125 (2012).
[7] M. Buoni and L. Petzold, J. Comput. Phys. **229**, 379 (2010).
[8] E. G. Flekkøy, Phys. Rev. E **47**, 4247 (1993).
[9] X. Shan and H. Chen, Phys. Rev. E **47**, 1815 (1993).
[10] X. Shan and H. Chen, Phys. Rev. E **49**, 2941 (1994).
[11] X. Shan, Phys. Rev. E **81**, 045701 (2010).
[12] E. Orlandini, M. R. Swift, and J. M. Yeomans, Europhys. Lett. **32**, 463 (1995).
[13] W. R. Osborn, E. Orlandini, M. R. Swift, J. M. Yeomans, and J. R. Banavar, Phys. Rev. Lett. **75**, 4031 (1995).
[14] M. R. Swift, E. Orlandini, W. R. Osborn, and J. M. Yeomans, Phys. Rev. E **54**, 5041 (1996).
[15] A. Lamura, G. Gonnella, and J. M. Yeomans, Europhys. Lett. **45**, 314 (1999).

[16] L.-S. Luo and S. S. Girimaji, Phys. Rev. E **67**, 036302 (2003).
[17] A. Xu, Europhys. Lett. **69**, 214 (2005).
[18] P. C. Facin, P. C. Philippi, and L. O. E. dos Santos, Future Gen. Comp. Syst. **20**, 945 (2004).
[19] P. Asinari, Phys. Fluids **17**, 067102 (2005).
[20] P. Asinari, Phys. Rev. E **73**, 056705 (2006).
[21] S. Arcidiacono, I. V. Karlin, J. Mantzaras, and C. E. Frouzakis, Phys. Rev. E **76**, 046703 (2007).
[22] P. Asinari, Phys. Rev. E **77**, 056706 (2008).
[23] P. Andries, K. Aoki, and B. Perthame, J. Stat. Phys. **106**, 993 (2002).
[24] F. A. Williams, *Combustion Theory*, 2nd ed. (Westview Press, Boulder, CO, 1994).
[25] P. Debye and E. Hückel, Phys. Z. **24**, 185 (1923).
[26] X. Liu, T. J. Vlugt, and A. Bardow, Fluid Phase Equilibr. **301**, 110 (2011).
[27] Chapman Thomas Woodring, Ph.D. thesis, University of California, Berkeley, 1967.
[28] Y. Sone, in *Advances in Kinetic Theory and Continuum Mechanics*, edited by R. Gatignol and Soubbaramayer (Springer, Berlin, 1991), pp. 19–31.
[29] M. Junk, A. Klar, and L. Luo, J. Comput. Phys. **210**, 676 (2005).
[30] R. B. Bird, W. E. Stewart, and E. N. Lightfoot, *Transport Phenomena* (John Wiley & Sons, New York, 1976).
[31] R. Taylor and K. R., *Multicomponent Mass Transfer*, Vol. 1 (Wiley-Interscience, New York, 1993).
[32] C. F. Curtiss and R. B. Bird, Industr. Eng. Chem. Res. **38**, 2515 (1999).
[33] R. B. Bird, W. E. Stewart, and E. N. Lightfoot, *Transport Phenomena*, 2nd ed. (John Wiley & Sons, New York, 2006).
[34] Cornelis Ronald Visser, Ph.D. thesis, Rijksuniversiteit Groningen, Groningen, 2001.
[35] G. Kraaijeveld and J. A. Wesselingh, Industr. Eng. Chem. Res. **32**, 738 (1993).
[36] R. Taylor and H. A. Kooijman, Chem. Eng. Commun. **102**, 87 (1991).
[37] C. W. Davies, *Ion Association* (Butterworths, London, 1962).
[38] K. Pitzer, *Activity Coefficients in Electrolyte Solutions* (Taylor & Francis, New York, 1991).
[39] X. Ge, X. Wang, M. Zhang, and S. Seetharaman, J. Chem. Thermodyn. **39**, 602 (2007).
[40] P. L. Bhatnagar, E. P. Gross, and M. Krook, Phys. Rev. **94**, 511 (1954).
[41] F. Millero, J. Ricco, and D. Schreiber, J. Solution Chem. **11**, 671 (1982).
[42] P. Asinari, Phys. Rev. E **80**, 056701 (2009).
[43] P. M. Mathias, Industr. Eng. Chem. Res. **43**, 6247 (2004).
[44] F. Golse, in *Handb. Diff. Equations*, edited by E. F. C. Dafermos, Vol. II (Elsevier-North-Holland, Amsterdam, 2005), pp. 159–301.
[45] I. Rubinstein and B. Zaltzman, Phys. Rev. E **62**, 2238 (2000).
[46] R. Kwak, V. S. Pham, K. M. Lim, and J. Han, Phys. Rev. Lett. **110**, 114501 (2013).
[47] X. He and L.-S. Luo, Phys. Rev. E **56**, 6811 (1997).
[48] P. J. Dellar, Comput. Math. Appl. **65**, 129 (2013).
[49] S. Brenner and L. Scott, *The Mathematical Theory of Finite Element Methods*, 2nd ed., Texts in Applied Mathematics (Springer-Verlag, Berlin, 2002).
[50] M. Gouy, J. Phys. Theor. Appl. **9**, 457 (1910).
[51] D. L. Chapman, Philos. Mag. Ser. 6 **25**, 475 (1913).
[52] M. Bazant, K. Chu, and B. Bayly, SIAM J. Appl. Math. **65**, 1463 (2005).